CLUSTERING DYNAMIC PET IMAGES ON THE GAUSSIAN DISTRIBUTED SINOGRAM DOMAIN

Mustafa E. Kamasak

Istanbul Technical University, Department of Computer Engineering, 34390, Istanbul, Turkey

ABSTRACT

Segmentation of dynamic PET images is an important preprocessing step for kinetic parameter estimation. The time activity curve (TAC) of individual pixels have very low signal-to-noise ratio (SNR). Therefore, the kinetic parameters estimated from these individual pixel TACs are not accurate, and these estimations may have very high spatial variance. To alleviate this problem, the pixels with similar kinetic characteristics are clustered into regions, and TACs of pixels within each region are averaged to increase the SNR. It is recently shown that it is better to cluster dynamic PET images in the sinogram domain than to cluster them in the reconstructed image domain [1]. In that study, the sinograms are assumed to have Poisson distribution. The clusters and TACs of the clusters are then chosen to maximize posterior probability of the measured sinograms. Although the raw sinogram data is Poisson distributed, the sinogram data that is corrected for scatter, randoms, attenuation etc. is not Poisson distributed anymore. The corrected sinogram data can be better described using Gaussian distribution. In this paper, we describe how to cluster dynamic PET images on the sinogram domain when the sinograms are Gaussian distributed.

1. INTRODUCTION

Positron emission tomography (PET) images generally have low signal-to-noise ratio (SNR) and the time activity curve (TAC) extracted from a single pixel may be very noisy. To improve the SNR, the TACs obtained from the physiologically similar pixels are averaged, and a single TAC is obtained for each group of pixels. Therefore, clustering physiologically similar pixels is an important preprocessing step. However, this is not a trivial task because of the low SNR and the partial volume effect of the PET images. In many PET studies, clustering is performed manually by an operator. Manual clustering is an operator dependent and time consuming process. For improved reproducibility and faster clustering various automatic clustering algorithms are developed.

Ashburner *et al.* [2] proposed a modified mixture model algorithm. This algorithm computes the likelihood of each pixel TAC being in a cluster and iteratively maximizes this likelihood. Wong *et al.* [3] proposed a distance based clustering algorithm. Weighted distance between the pixel TACs within each cluster is minimized. This algorithm is further described in section 3.1. Chen *et al.* [4] used an expectation maximization (EM) based clustering algorithm with Markov random field (MRF) models. Brankov *et al.* [5] proposed a new distance metric between the pixel TACs and iteratively minimizes this distance within the pixel TACs of each cluster. Automatic clustering can also be integrated into kinetic parameter estimation algorithms [6]. In some studies, segmentation is used to estimate the plasma input function from the PET images without arterial sampling [7, 8].

These clustering algorithms generally use pixel TACs as their feature vectors, which require reconstructed dynamic PET images. Sinogram data acquired with PET scanners are reconstructed using conventional tomographic reconstruction algorithms and TACs are extracted from these reconstructed images. In this paper, we extend our Poisson distributed sinogram domain clustering algorithm for the Gaussian distributed sinograms.

2. UNSUPERVISED CLUSTERING ON PROJECTION DOMAIN

This section describes the unsupervised clustering algorithm on the projection domain. We introduce some notation, give some brief information on the scanner model, and then describe our MAP framework.

Assume that the data is collected at K time frames, and there are L clusters in the image. Each cluster has an associated TAC and a set of pixels that belongs to this cluster. For cluster l, let $\mu_l = [\mu_{l0}, \cdots, \mu_{l(K-1)}]$ denote the TAC of the cluster, and let Ω_l denote the set of pixels that belongs to this cluster. Let μ denote $L \times K$ matrix formed as $\mu = [\mu_0, \mu_1, \cdots, \mu_{L-1}]^T$ where superscript T denotes the matrix transpose. Let Ω denote the label image, ie. $\Omega = \{\Omega_0, \cdots, \Omega_{L-1}\}$.

Given the sinogram measurements, denoted by Y, the MAP estimates of μ and Ω are

$$(\mu, \Omega) \leftarrow \arg\max p(\mu, \Omega | Y) \ , \tag{1}$$

where $p(\cdot)$ denotes the probability.

In the following sections, we formulate $p(Y|\mu,\Omega)$ when Y is Gaussian distributed and then we describe how to estimate (μ,Ω) iteratively and efficiently.

2.1 Scanner Model

Let Y_{mk} denote the sinogram measurement for projection $0 \le m < M$ and time frame $0 \le k < K$, and let Y be the $M \times K$ matrix of independently distributed Poisson random variables that form the sinogram measurements. Furthermore, let A be the forward projection matrix, with elements A_{ms}. A_{ms} denotes the probability of an emission from pixel s being detected by the m^{th} detector pair. Then, the expected number of counts for each measurement at a given time, t_k is given by

$$E[Y_{mk}|\mu,\Omega] = \sum_{l=0}^{L-1} \sum_{s \in \Omega_l} A_{ms}\mu_{lk} \ . \tag{2}$$

For simplicity of notation let's define

$$Q_{ml}(\Omega) = \sum_{s \in \Omega_l} A_{ms} \ , \tag{3}$$

$$Q_m(\Omega) = [Q_{m0}, \cdots, Q_{m(L-1)}] \ , \tag{4}$$

and

$$Q(\Omega) = \begin{bmatrix} Q_0 \\ \vdots \\ Q_{M-1} \end{bmatrix} \tag{5}$$

Then equation (2) can be compactly expressed in the matrix notation as

$$E[Y|\mu,\Omega] = Q(\Omega)\mu \ . \tag{6}$$

If we assume that the sinogram data is composed of independent Poisson distributed measurements, the probability density function for the measured sinogram is

$$p(Y|\mu,\Omega) = \prod_{k=0}^{K-1} \prod_{m=0}^{M-1} \frac{(Q_m(\Omega)\mu_{*k})^{Y_{mk}} e^{-(Q_m(\Omega)\mu_{*k})}}{Y_{mk}!} \tag{7}$$

where μ_{*k} is the k^{th} column of μ.

However, if the sinogram is corrected for scatter, randoms, attenuation etc., then the sinogram data can better described using Gaussian distribution. In this case, the probability density function for the measured sinogram becomes

$$p(Y|\mu,\Omega) = \prod_{k=0}^{K-1}\prod_{m=0}^{M-1} \frac{1}{\sqrt{2\pi}\sigma_{mk}} \exp\left\{ \frac{-1}{2\pi\sigma_{mk}^2}(Y_{mk} - Q_m(\Omega)\mu_{*k})^2 \right\} \tag{8}$$

where σ_{mk} is the standard deviation of Y_{mk}.

2.2 Estimation Framework

A cost function can be formed by negating the logarithm of the probability density function given in (8) and adding a regularization function, $S(\Omega)$.

$$C(Y|\mu,\Omega) = -ln\left(p(Y|\mu,\Omega)\right) + S(\Omega) \tag{9}$$

The regularization function penalizes the local label changes and therefore it controls the spatial continuity of pixel labels. This type of regularizaton function was used by Besag [9] for image clustering.

The regularization function can be obtained from an assumed prior distribution of the label image. In this work, we model the label image as a Markov random field (MRF) with Gibbs distribution. The likelihood of a particular label image, Ω is then

$$p(\Omega) = \frac{1}{Z}\exp\left\{ -\beta \sum_{s,r\in\mathcal{N}} g_{s-r}(1-\delta(\omega_s,\omega_r)) \right\}, \tag{10}$$

where Z is the normalization constant, $\mathcal{N}$ is the set of all spatially neighboring pixel pairs in Ω, g_{s-r} is the coefficient linking pixels s and r, β is a constant that controls the spatial smoothness of the label image, and $\delta(\cdot,\cdot)$ denotes the Kronecker delta function.

In this paper, $\mathcal{N}$ is formed by 8-point spatial neighborhood. We choose the negative logarithm of (10) as our regularization function, ie.

$$S(\Omega) = \beta \sum_{s,r\in\mathcal{N}} g_{s-r}(1-\delta(\omega_s,\omega_r)) \,. \tag{11}$$

Note that with this regularization function, high values of the regularization parameter, β, will correspond to spatially smoother label images. We can similarly add another regularization function for the temporal smoothness of the cluster TACs.

The labels and region TACs are assigned to minimize the cost function given in (9)

$$\Omega,\mu \leftarrow \arg\min C(Y|\Omega,\mu) \,. \tag{12}$$

2.3 Clustering with Iterative Coordinate Descent Clustering (CICD)

An iterative coordinate-descent minimization technique is used to minimize (9). This algorithm is named as "clustering with iterative coordinate descent (CICD). A CICD iteration has two steps; first the cluster TACs are fixed and pixel labels are sequentially updated to minimize the cost function. When all pixel labels are updated, the cluster TACs are updated to minimize the cost function. Therefore, with each CICD iteration, the cost function monotonically decreases.

2.3.1 Pixel Label Update

First, all cluster TACs are fixed and pixel labels are updated. Let ω_s denote the current label of pixel s, and we want to change it to be $\tilde{\omega}_s$ in this iteration so that the change in the cost function is minimized. If we change the label of pixel s from ω_s to $\tilde{\omega}_s$, the change in the cost function is

$$\begin{aligned}\Delta C(Y|\omega_s,\tilde{\omega}_s) &= C(Y|\omega_s) - C(Y|\tilde{\omega}_s) \\ &= ln(p(Y|\tilde{\omega}_s)) - ln(p(Y|\omega_s)) \\ &\quad + \beta \sum_{r\in\partial s} g_{s-r}(1-\delta(\tilde{\omega}_s,\omega_r))\end{aligned} \tag{13}$$

where

$$\begin{aligned}&ln(p(Y|\tilde{\omega}_s) - ln(p(Y|\omega_s)) = \\ &\qquad \sum_{k=0}^{K-1}\sum_{m=0}^{M-1} \frac{A_{ms}(-2(Y_{mk} - Q_m(\Omega)) + A_{ms}(\mu_{\tilde{\omega}_s k} - \mu_{\omega_s k}))}{\sigma_{mk}^2}\end{aligned} \tag{14}$$

and ∂s denotes the set of pixels that are neighbors of pixel s. Since A is a sparse matrix, there will be few nonzero terms in (14).

Then the label of each pixel is updated as

$$\tilde{\omega}_s \leftarrow \arg\min \Delta C(Y|\omega_s,\tilde{\omega}_s) \tag{15}$$

This minimization is performed by simply searching through all possible (L) values of $\tilde{w}_s$. For efficient implementation, $\{Q_{ml}\}_{l=0}^{L-1}$ can be stored in the memory. Whenever a pixel label is updated $\{Q_{ml}\}_{l=0}^{L-1}$ can also be updated as follows

$$\begin{aligned} Q_{m\omega_s} &\leftarrow Q_{m\omega_s} - A_{ms} \\ Q_{m\tilde{\omega}_s} &\leftarrow Q_{m\tilde{\omega}_s} + A_{ms} \text{ for } m = 0\cdots M-1 \,. \end{aligned} \tag{16}$$

2.3.2 Cluster TAC update

Once all the pixel labels are updated, we can update the cluster TACs. The cluster TACs are also updated as follows to minimize the cost function given in (9). Since the cost function is quadratic in terms of μ, there is a closed form expression for the update of cluster TACs. The first and second derivative of the cost function with respect to μ_{lk} are

$$\frac{d}{d\mu_{lk}}C(Y|\mu) = -2\sum_{m=0}^{M-1}\frac{Q_{ml}(Y_{mk} - Q_m(\Omega)\mu_{*k})}{\sigma_{mk}^2} \tag{17}$$

and

$$\frac{d^2}{d{\mu_{lk}}^2}C(Y|\mu) = 2\sum_{m=0}^{M-1}\frac{Q_{ml}^2}{\sigma_{mk}^2} \,. \tag{18}$$

If we define the gradient and hessian of the cost function as

$$\nabla_{\mu_l} = \begin{bmatrix} \frac{d}{d\mu_{l0}}C(Y|\mu) \\ \frac{d}{d\mu_{l1}}C(Y|\mu) \\ \vdots \\ \frac{d}{d\mu_{l(K-1)}}C(Y|\mu) \end{bmatrix} \tag{19}$$

$$\nabla^2_{\mu_l} = diag\left\{ \frac{d^2}{d{\mu_{l0}}^2}C(Y|\mu), \frac{d^2}{d{\mu_{l1}}^2}C(Y|\mu), \cdots, \frac{d^2}{d{\mu_{l(K-1)}}^2}C(Y|\mu) \right\}, \tag{20}$$

then the new cluster TAC, $\tilde{\mu}_l$, can be computed as follows

$$\tilde{\mu}_l = \mu_l - (\nabla^2_{\mu_l})^{-1}\nabla_{\mu_l} \,. \tag{21}$$

3. IMAGE-DOMAIN CLUSTERING ALGORITHMS

Image domain clustering algorithms use TACs extracted from emission images. The emission images are reconstructed using conventional PET reconstruction algorithms. Let x_{sk} be the reconstructed emission rate for pixel s at time frame k, and $x_s = [x_{s0},\cdots,x_{s(K-1)}]$ be the reconstructed time response of pixel s.

3.1 Weighted Least Squares Clustering (WLS)

This algorithm minimizes the weighted square distance between the pixel TACs and the cluster TACs, ie.

$$(\mu,\Omega) \leftarrow \arg\min_{\mu,\Omega} \sum_{l=0}^{L-1}\sum_{s\in\Omega_l} \|x_s - \mu_l\|^2_W \,, \tag{22}$$

where W is a weight matrix, and $\|x\|_W^2$ denotes $x^T W x$. In this work we used a diagonal weighting matrix formed as $W = diag\{\Delta t_k\}_{k=0}^{K-1}$ where Δt_k is the duration of k^{th} time frame.

This algorithm also iteratively updates the pixel labels and cluster TACs. Each iteration consists of two steps. In the first step, labels of pixels are sequentially updated. The label of a pixel is updated as follows

$$\tilde{\omega}_s \leftarrow \arg\min_l \|x_s - \mu_l\|_W^2 \tag{23}$$

After all pixel labels are updated, the cluster TACs are updated as follows to decrease the weighted distance given in (22).

$$\mu_l = \frac{1}{|\Omega_l|} \sum_{s \in \Omega_l} x_s \ , \tag{24}$$

where $|\Omega_l|$ denotes the number of pixels that are labeled as l. Each WLS iteration monotonically decreases the cost function, and iterations are repeated until the stopping (convergence) criteria is reached.

3.2 Gaussian Mixture Model with Expectation Maximization (GMM-EM)

It can be assumed that the pixel TACs are Gaussian distributed around the cluster TACs. Similar to other clustering methods pixel labels and cluster TACs can be updated iteratively.

Let R_l denote the covariance matrix of cluster l, and π_l denote the probability of cluster l. The posterior probability of a pixel being in cluster l, given its time response is

$$p(\omega_s = l | x_s, \mu_l) = \frac{\pi_l}{(2\pi)^{K/2}} |R_l|^{-1/2} \exp\left\{ -\frac{1}{2}(x_s - \mu_l)^T R_l^{-1} (x_s - \mu_l) \right\} \tag{25}$$

If the TACs and covariance matrices of the clusters are known, we can assign pixel labels to maximize the posterior, ie.

$$\omega_s \leftarrow \arg\min_l \left\{ \frac{1}{2}(x_s - \mu_l)^T R_l^{-1} (x_s - \mu_l) + \frac{1}{2}\log|R_l| - \log(\pi_l) \right\} \tag{26}$$

Once the labels are assigned the cluster TACs and covariance matrices can be updated using the EM algorithm [10].

4. SIMULATIONS

4.1 Phantom Design

Simulation experiments are based on a phantom of a rat's head. The phantom and kinetic parameters for the regions in this phantom are taken from Kamasak *et al* [11]. Figure 1 shows a schematic representation of the phantom and its regions. The phantom has six regions including the background. The regional TACs are shown in figure 2. For further details about the phantom see Kamasak *et al* [11]. Time frames of emission images are generated using the phantom and the 2-tissue compartment model equations. The plasma function, $C_P(t)$, is generated using the second model in Wong *et al* [12]. The blood contribution to the PET activity is assumed to be zero, and the tracer is assumed to be raclopride labeled with ^{11}C, which has a decay constant of $\lambda = 0.034$ min^{-1}. Total scan time is 60 min., divided into 18 time frames with 4×0.5 min, 4×2 min, and 10×5 min. The phantom resolution is 128×128 with each pixel having dimensions of (1.2 mm)^2. The data is not decay-corrected.

The rat phantom image at each time frame is forward projected into sinograms using a Poisson model for the detected counts. Each sinogram consists of 180 angles and 200 radial bins per angle. A triangular point spread function with a 4 mm base width is used in forward projections.

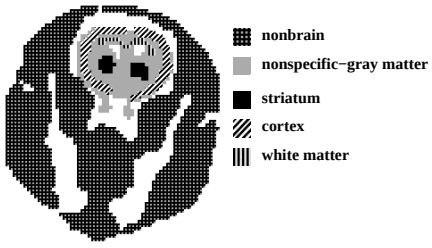

Figure 1: Single-slice rat phantom. Regions of the rat phantom were derived from a segmented MR image. Different fill patterns indicate kinetically distinct tissue regions.

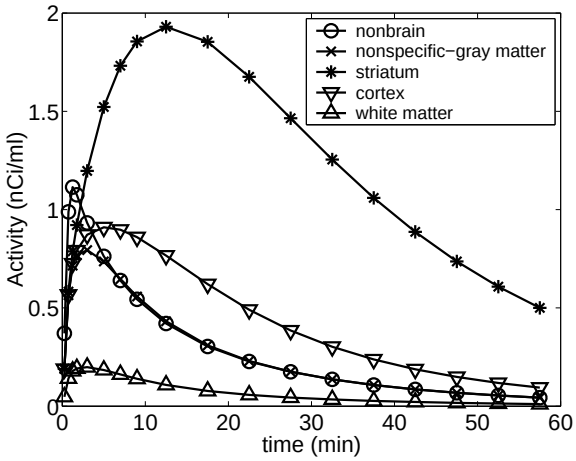

Figure 2: Simulated time-activity curves for 5 distinct tissue regions in rat brain phantom.

The image-domain clustering algorithms of Section 3 require that the emission images be reconstructed for each time frame. We used ICD image reconstruction with a quadratic prior and a regularization parameter for each time frame [13]. The regularization parameters were chosen to minimize the total mean square error of the reconstructed emission image frames.

Both the CICD and image-domain clustering algorithms are stopped when none of the pixels change label during an iteration.

4.2 Performance Evaluation

Clustering algorithms are evaluated based on their performance of labeling pixels and estimating the cluster TACs. Two seperate performance measures are used: Misclassification percentage and RMSE of the cluster TACs.

Misclassification percentage, given in (27), is used to evaluate the labeling performance of the clustering algorithms. Misclassification percentage is computed as

$$\text{misclassification } (\%) = \frac{100}{N} \sum_{s=1}^{N} (1 - \delta(\omega_s^{estimated}, \omega_s^{original})) \ . \tag{27}$$

In (27), $\omega_s^{estimated}$ denotes the label of pixel s assigned by the proposed clustering algorithm, and $\omega_s^{original}$ denotes the correct label of pixel s.

The RMSE, given in (28), is used to evaluate the accuracy of the cluster TACs estimated by the clustering algorithms. The RMSE of the TAC estimations is computed as

$$\text{RMSE} = \sqrt{\frac{1}{K} \sum_{l=1}^{L} \|\mu_l^{estimated} - \mu_l^{original}\|^2} \ . \tag{28}$$

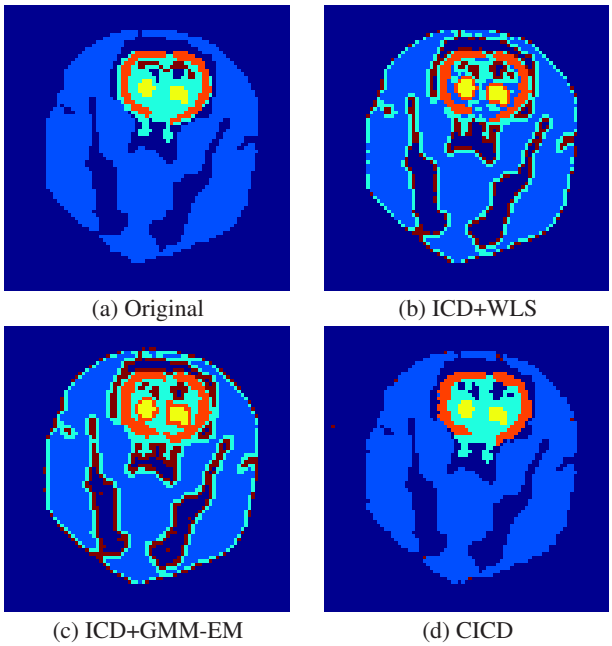

(a) Original (b) ICD+WLS

(c) ICD+GMM-EM (d) CICD

Figure 3: Pixel labels assigned by the clustering algorithms.

method	misclassification (%)
ICD + WLS	5.41
ICD + GMM	6.23
CICD	0.68

Table 1: Percentage of mislabeled pixels for the clustering algorithms.

In (28), $\mu_l^{estimated}$ denotes the TAC for cluster l estimated by the proposed clustering algorithm, and $\mu_l^{original}$ is the correct TAC for cluster l.

5. SIMULATION RESULTS

The pixel labels assigned by the image-domain algorithms and the proposed method, CICD, are shown in figure 3. The images are clustered into six regions that are shown in figure 1. For these simulations, the regularization parameter, β, is set to fifty. This parameter is chosen empirically to minimize the misclassification percentage.

Visually it can be seen that CICD algorithm results have less mislabeled pixels than image-domain clustering methods. The percentage of mislabeled pixels for these algorithms are computed using (27) and given in table 1. From this table, it can be seen that the proposed clustering algorithm has the lowest mislabeled pixel percentage.

The cluster TACs estimated by the clustering algorithms are shown in figure 4. The root mean squared error for the cluster TACs are computed using (28) and listed in table 2. This table shows that for all regions except the white matter and nonbrain, the proposed algorithm have produced the lowest root mean squared error (RMSE) between the estimated cluster TACs and the actual cluster TACs.

The success of the proposed CICD algorithm is due to the reduction in the number of estimated parameters. CICD algorithm assigns N labels and estimates $L \times K$ time points for cluster TACs. However, for image-domain clustering algorithms, the estimation of additional $N \times K$ emission rates for reconstructed emission images is required.

region	WLS	GMM-EM	CICD
background	0.017	0.022	**0.000**
nonbrain	0.013	**0.007**	0.013
nonspecific-gray matter	0.088	0.092	**0.022**
striatum	0.207	0.239	**0.033**
cortex	0.059	0.088	**0.025**
white matter	0.059	**0.019**	0.838

Table 2: RMSE of the cluster TACs for each region in the rat's head.

6. CONCLUSION

We proposed a new clustering algorithm that we call clustering with iterative coordinate descent [1]. CICD clusters the dynamic PET images directly on the projection domain, and it does not require the intermediate step of emission reconstruction. The CICD algorithm produces less mislabeled pixels and estimates cluster TACs generally with lower RMSE than the image-domain clustering algorithms.

In this paper, we extend this algorithm for the case where the projection data is Gaussian distributed. We obtain similar results to our CICD algorithm with Poisson distributed sinograms.

REFERENCES

[1] M. E. Kamasak and B. Bayraktar, "Clustering dynamic PET images on the projection domain," *IEEE Trans. on Nuclear Science*, 2007, (accepted).

[2] J. Ashburner, J. Haslam, C. Taylor, V. J. Cunningham, and T. Jones, "A cluster analysis approach for the characterization of dynamic PET data," in *Quantification of Brain Function Using PET*, R. Myers, V. Cunningham, D. Bailey, and T. Jones, Eds. San Diego: Academic Press, 1996, pp. 301–306.

[3] K.-P. Wong, D. Feng, S. R. Meikle, and M. J. Fulham, "Segmentation of dynamic PET images using cluster analysis," *IEEE Trans. on Nuclear Science*, vol. 49, no. 1, pp. 200–207, 2002.

[4] J. L. Chen, S. R. Gunn, M. S. Nixon, and R. N. Gunn, "Markov random field models for segmentation of PET images," in *Proceedings of Information Processing in Medical Imaging 2082*, 2001, pp. 468–474.

[5] J. G. Brankov, N. P. Galatsanos, Y. Yang, and M. N. Wernick, "Segmentation of dynamic PET or fMRI images based on a similarity metric," *IEEE Trans. on Nuclear Science*, vol. 50, no. 5, pp. 1410–1414, 2003.

[6] Y. Kimura, M. Senda, and N. Alpert, "Fast formation of statistically reliable FDG parametric images based on clustering and principal components," *Phys. Med. Biol.*, vol. 47, pp. 455–468, August 2002.

[7] M. Liptrot, K. H. Adams, L. Martiny, L. H. Pinborg, M. N. Lonsdale, N. V. Olsen, S. Holm, C. Svarer, and G. M. Knudsen, "Cluster analysis in kinetic modelling of the brain: a noninvasive alternative to arterial sampling," *NeuroImage*, vol. 21, no. 2, pp. 483–493, 2004.

[8] K.-P. Wong, D. Feng, S. R. Meikle, and M. J. Fulham, "Noninvasive extraction of physiological parameters in quantitative PET studies using simultaneous estimation and cluster analysis," in *Proceedings of IEEE Medical Imaging Conference*, Lyon, France, October 2000, pp. 141–145.

[9] J. Besag, "On the statistical analysis of dirty pictures," *Journal of the Royal Statistical Society B*, vol. 48, no. 3, pp. 259–302, 1986.

[10] A. P. Dempster, N. M. Laird, and D. B. Rubin, "Maximum likelihood from incomplete data via the EM algorithm," *Jour-*

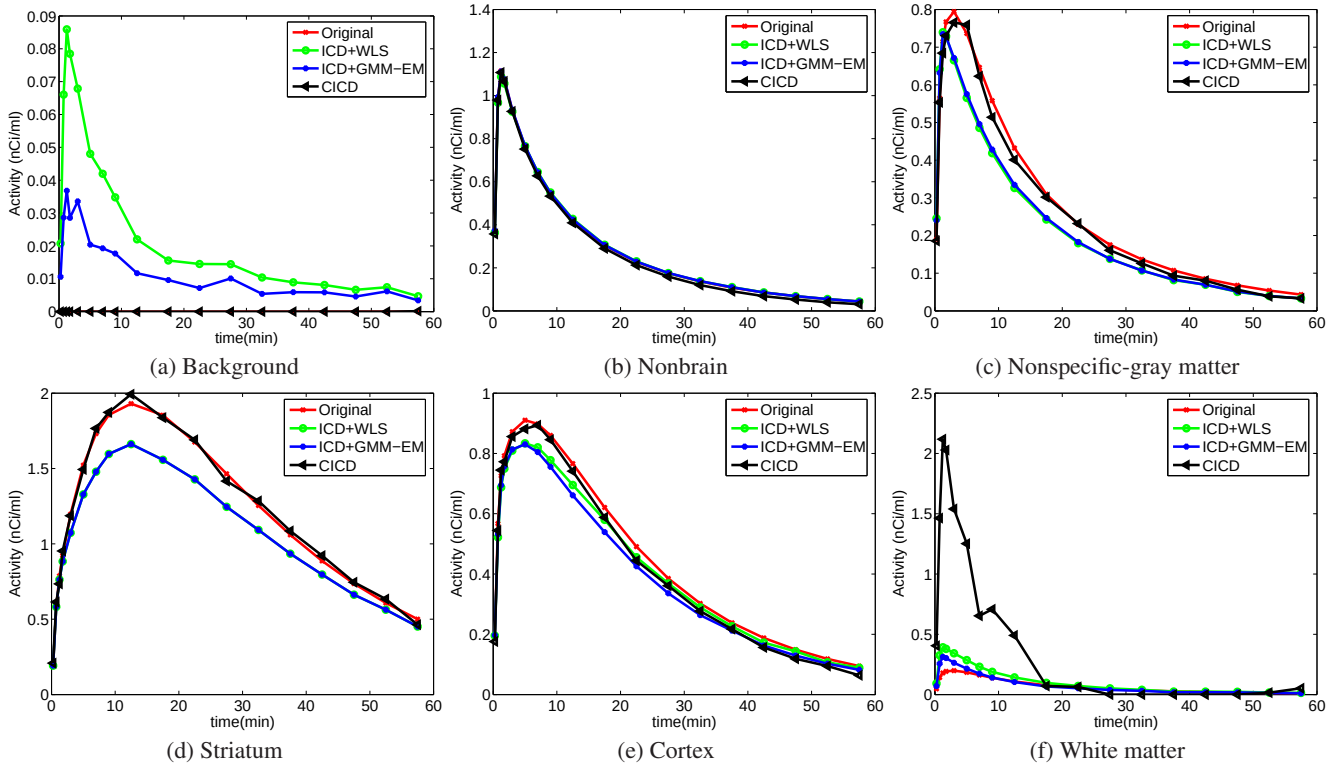

(a) Background (b) Nonbrain (c) Nonspecific-gray matter

(d) Striatum (e) Cortex (f) White matter

Figure 4: Cluster TACs estimated by the clustering algorithms for each region in the rat head.

nal of the Royal Statistical Society B, vol. 39, no. 1, pp. 1–38, 1977.

[11] M. E. Kamasak, C. A. Bouman, E. D. Morris, and K. Sauer, "Direct reconstruction of kinetic parameter images from dynamic PET data," *IEEE Trans. on Medical Imaging*, vol. 24, no. 5, pp. 636–650, May 2005.

[12] K.-P. Wong, D. Feng, S. R. Meikle, and M. J. Fulham, "Simultaneous estimation of physiological parameters and the input function - in *vivo* PET data," *IEEE Transactions on Information Technology in Biomedicine*, vol. 5, no. 1, pp. 67–76, March 2001.

[13] C. A. Bouman and K. Sauer, "A unified approach to statistical tomography using coordinate descent optimization," *IEEE Trans. on Image Processing*, vol. 5, no. 3, pp. 480–492, March 1996.